

# GALAXY MAPPING WITH THE SAURON INTEGRAL-FIELD SPECTROGRAPH: THE STAR FORMATION HISTORY OF NGC 4365

ROGER L. DAVIES<sup>1</sup>, HARALD KUNTSCHNER<sup>1</sup>, ERIC EMSLEEM<sup>2</sup>, R. BACON<sup>2</sup>,  
M. BUREAU<sup>3</sup>, C. MARCELLA CAROLLO<sup>4</sup>, Y. COPIN<sup>2</sup>, BRYAN W. MILLER<sup>3,5</sup>, G. MONNET<sup>6</sup>,  
REYNIER F. PELETIER<sup>1,7</sup>, E.K. VEROLME<sup>3</sup>, P. TIM DE ZEEUW<sup>3</sup>

<sup>1</sup> University of Durham, Department of Physics, South Road, Durham DH1 3LE, UK

<sup>2</sup> CRAL - Observatoire de Lyon, 9 Avenue Charles-André, 69230 Saint-Genis-Laval, France

<sup>3</sup> Sterrewacht Leiden, Niels Bohrweg 2, 2333 CA Leiden, The Netherlands

<sup>4</sup> Department of Astronomy, Columbia University, 538 West 120th Street, New York, NY 10027, USA

<sup>5</sup> Gemini Observatory, Casilla 603, La Serena, Chile

<sup>6</sup> European Southern Observatory, Karl-Schwarzschild Straße 2, 85748 Garching, Germany

<sup>7</sup> Dept. of Physics & Astronomy, Univ. of Nottingham, University Park, Nottingham NG7 2RD, UK

*Draft version October 31, 2018*

## ABSTRACT

We report the first wide-field mapping of the kinematics and stellar populations in the E3 galaxy NGC 4365. The velocity maps extend previous long-slit work. They show two independent kinematic subsystems: the central  $300 \times 700$  pc rotates about the projected minor axis, and the main body of the galaxy,  $3 \times 4$  kpc, rotates almost at right angles to this. The line-strength maps show that the metallicity of the stellar population decreases from a central value greater than solar, to one-half solar at a radius of 2 kpc. The decoupled core and main body of the galaxy have the same luminosity-weighted age, of  $\approx 14$  Gyr, and the same elevated magnesium-to-iron ratio. The two kinematically distinct components have thus shared a common star formation history. We infer that the galaxy underwent a sequence of mergers associated with dissipative star formation that ended  $\gtrsim 12$  Gyr ago. The misalignment between the photometric and kinematic axes of the main body is unambiguous evidence of triaxiality. The similarity of the stellar populations in the two components suggests that the observed kinematic structure has not changed substantially in 12 Gyr.

*Subject headings:* galaxies: abundances — galaxies: elliptical and lenticular — galaxies: evolution — galaxies: formation — galaxies: individual (NGC 4365) — galaxies: kinematics and dynamics — galaxies: stellar content

## 1. INTRODUCTION

The existence of decoupled cores in  $\approx 30\%$  of the early-type galaxies is strong evidence that mergers play an important part in the evolution of these systems (e.g., de Zeeuw & Franx 1991). Most likely, decoupled cores originate from the accretion of material with angular momentum misaligned from that of the main galaxy. A few galaxies have been studied in sufficient detail to explore when that material was accreted or whether the event was associated with gaseous dissipation and star formation. For example in the morphologically normal galaxies IC 1459 (Franx & Illingworth 1988) and NGC 5322 (Bender 1988; Rix & White 1992) there is no difference between the colors or line-strengths of the stellar populations in the decoupled core and the main galaxy. In contrast, the disturbed shell galaxy NGC 2865 shows evidence for very recent star formation in the decoupled component (Hau, Carter, & Balcells 1999).

NGC 4365 is one of the first elliptical galaxies in which minor axis rotation was discovered (Wagner, Bender, & Möllenhoff 1988; Bender, Saglia, & Gerhard 1994). Surma & Bender (1995, hereafter SB) deduced the remarkable kinematic structure of NGC 4365 from three long-slit spectra. The main body of the galaxy rotates around its *major* axis, reaching a maximum velocity of  $\approx 50$  km s $^{-1}$ , whereas at smaller radii ( $r = 2\text{--}3''$ ) the peak rotation velocity is 80 km s $^{-1}$  around the *minor* axis. SB found that the

decoupled core is flatter than the main galaxy (ellipticity  $\varepsilon_{\text{core}}=0.39$  cf.  $\varepsilon_{\text{main}}=0.23$ ). By carrying out a careful double Gaussian analysis of the kinematics, SB estimate that  $V/\sigma = 1.3$  for the core, consistent with a disk or bar. They deduced that the rotating core contributes 25% of the light within  $r \approx 6''$ , and accounts for roughly 2% of the *total* mass. The giant elliptical galaxy in which it is embedded has a central velocity dispersion of 275 km s $^{-1}$ . They found that the decoupled core contains a high-metallicity population, with an enhanced [Mg/Fe] ratio as commonly found in giant ellipticals. SB concluded that NGC 4365 is triaxial, and that the formation of the core involved substantial gaseous dissipation and star formation. However, they could not distinguish formation scenarios where the merger(s) occur early ( $z > 2\text{--}3$ ) from those where the mergers occur more recently ( $z < 1$ ).

HST images reveal that NGC 4365 has a smooth intensity profile with no signs of dust, an average ellipticity of 0.26, and a very shallow central cusp. The isophotes are disky for  $1'' < r < 4''$  and boxy at larger radii. At the very centre ( $r \lesssim 0''.2$ ) there is a blue point source (van Dokkum & Franx 1995; Carollo et al. 1997). Deep ground-based images show no evidence for shells or other morphological peculiarities out to  $\approx 4 r_e$  (Blakeslee, private communication).

Surface-brightness-fluctuation measurements indicate that NGC 4365 is in the Virgo W cloud beyond the main

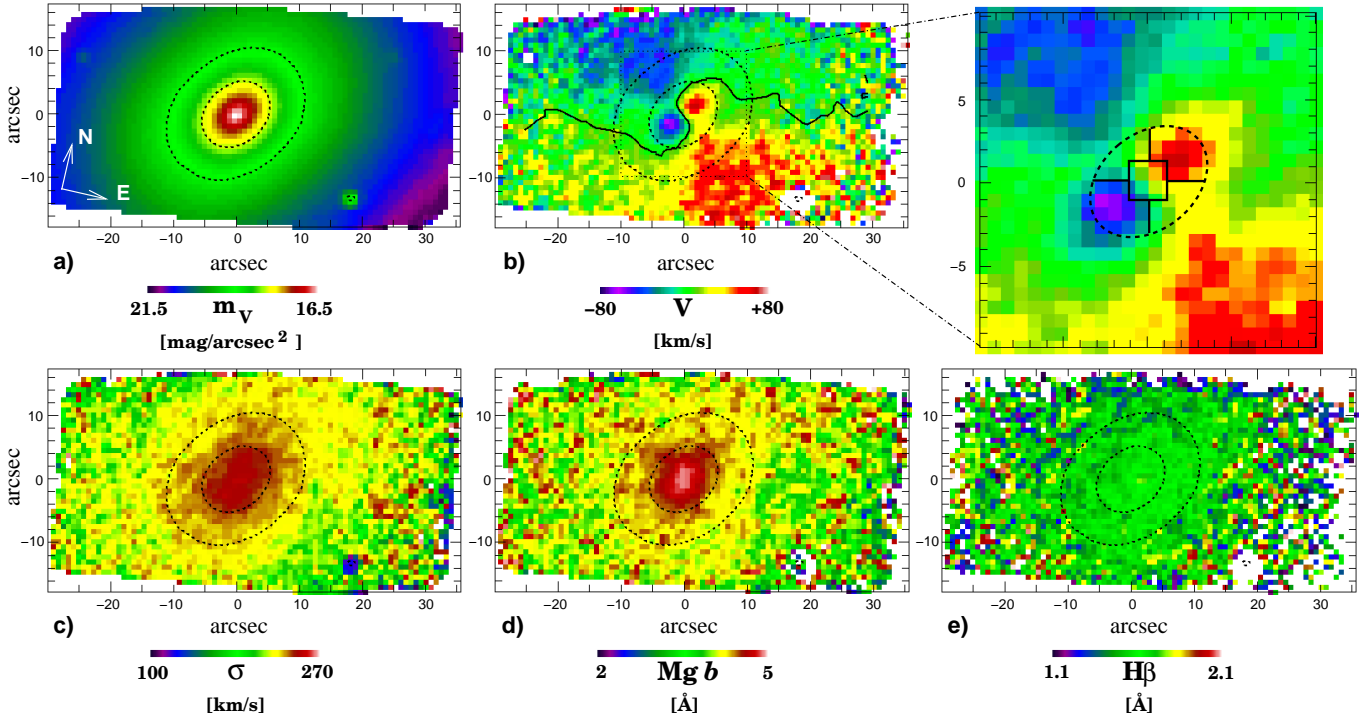


FIG. 1.— Maps of a) surface brightness as reconstructed from our data, b) mean streaming velocity  $V$ , c) velocity dispersion  $\sigma$ , d)  $Mg\,b$  line-strength, and e)  $H\beta$  line-strength, for NGC 4365. The maps are based on two partially overlapping SAURON pointings of  $4 \times 1800$  s each, sampled with  $0''.8 \times 0''.8$  pixels. Isophotal contours of  $\mu_V = 18$  and  $19$  mag/arcsec $^2$  are overplotted in panels (a) to (e) (dashed lines). A zero-velocity contour line (solid black line) is shown in panel (b). The enlarged core region of the velocity map indicates the regions which we have used for our line-strength analysis: The central point is indicated by the square, the decoupled core by the sectors along the major axis and the main body at the same radius by the sectors along the minor axis.

cluster (Jensen, Tonry, & Luppino 1998). We take the distance modulus to be 31.7 mag, a distance of 22 Mpc, so that  $1''$  is  $\approx 100$  pc. The effective radius  $r_e$  is  $57''$ , or  $\approx 5.7$  kpc (Burstein et al. 1987).

In this Letter, we present the first complete maps of the kinematics and stellar populations of NGC 4365, taken with the wide-field integral-field spectrograph SAURON (Bacon et al. 2001). In §2, we briefly describe the observations. The kinematics and line-strength index maps are presented in §3, where we consider age-metallicity diagnostics, the  $Mg-\sigma$  diagram, and the spatial distribution of non-solar abundance ratios. We discuss the implications of these results for formation scenarios in §4, and summarize our conclusions in §5.

## 2. OBSERVATIONS

We observed NGC 4365 with SAURON mounted on the 4.2m William Herschel Telescope on La Palma, on the nights of 29 & 30 March 2000. SAURON has a field-of-view of  $33'' \times 41''$ , delivering simultaneously 1431 spectra at a spectral resolution of  $3.6$  Å (FWHM),  $0''.95 \times 0''.95$  spatial sampling, and 100% sky coverage (Bacon et al. 2001). Another 146 spectra are taken  $1''.9$  away from the main field, to allow accurate sky subtraction. The wavelength range of the current setup is  $\approx 4810$ – $5350$  Å. We observed two fields overlapping by  $\approx 20''$  on the nuclear region of NGC 4365, each field having four separate exposures of 1800 s (dithered by  $\approx 1''$ , i.e., one lenslet). The combined datacubes cover a total region of  $33'' \times 63''$  on the sky. The small offsets between the four 1800 s integrations at each position enable us to re-sample the final datacubes

onto  $0''.8 \times 0''.8$  pixels (drizzling technique). The seeing of the merged datacube was measured on three point-like objects in the reconstructed image. It is homogeneous over the field with a value of  $1''.6 \pm 0''.1$  (FWHM). We took arc-lamp spectra before and after each individual exposure for accurate wavelength calibration.

We reduced the raw SAURON exposures by means of the algorithms described in Bacon et al. (2001). We used the individually-extracted, wavelength-calibrated and continuum-corrected spectra to derive the stellar kinematics and line-strength indices as a function of (two-dimensional) position in NGC 4365. We measured the mean velocity  $V$  and the velocity dispersion  $\sigma$  with the Fourier Correlation Quotient method (Bender 1990), and obtained the line-strength indices  $H\beta$ ,  $Mg\,b$  and  $Fe5270$  in the Lick/IDS system (Worthey 1994), taking into account the internal velocity broadening and differences in the instrumental resolution.

## 3. RESULTS

Figure 1a shows the surface brightness distribution of NGC 4365, as reconstructed from our spectra. The reconstructed intensity map agrees well with the HST image after seeing convolution and binning to the SAURON spatial sampling.

Figure 1b shows the spectacular kinematically decoupled core of NGC 4365 in detail. The core extends  $\approx 7'' \times 3''$  and rotates about the minor axis. The maximum observed core rotation speed is  $80$  km s $^{-1}$  at a radius of  $2''.2$ . The main body of the galaxy rotates slowly about an axis misaligned by  $8 \pm 2^\circ$  with the major axis. The rotation velocity

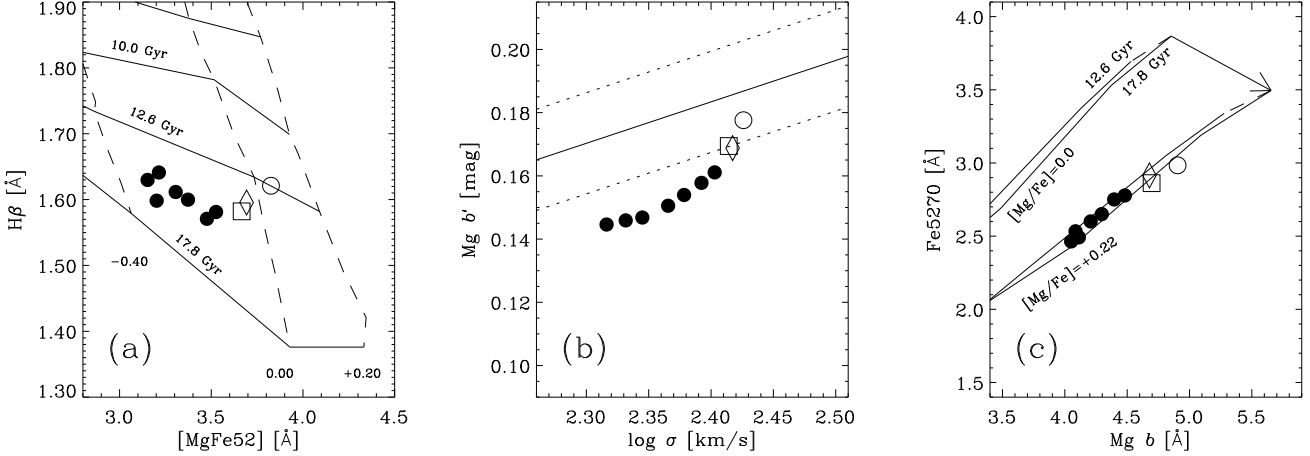


FIG. 2.— (a)  $[\text{MgFe52}]$  vs  $\text{H}\beta$  equivalent width diagram. The open circle represents the average line-strength of the very central data points ( $r < 1''.6$ ), the open diamond represents the region of the decoupled core, and the open square reflects the mean of the data in the main body of the galaxy at the same radii as the decoupled core (see also Figure 1, enlarged core region). For larger radii, the data was averaged in elliptical annuli centered on the photometric nucleus (filled circles); mean semi-major axis radii: 5.6, 7.2, 9.6, 12.9, 16.0, 19.9 & 26.1'' (radius increases from right to left). Overplotted are the predictions of stellar population models from Vazdekis (1999). The solid lines are lines of constant age and the dashed lines are lines of constant metallicity ( $[\text{M}/\text{H}]$ ). (b) Local velocity dispersion vs local  $\text{Mg } b'$  index. The solid line indicates the average relation for the cores of early-type galaxies (Colless et al. 1999) and the dashed lines indicate the  $1\sigma$  spread around it. (c)  $\text{Mg } b$  vs  $\text{Fe5270}$  equivalent width diagram. Overplotted are stellar population models from Vazdekis (1999) with solar abundance ratios for an age of 12.6 & 17.8 Gyrs. Additionally a correction of the models for *non-solar* abundance ratios of  $[\text{Mg/Fe}] = +0.22$  dex is shown (Trager et al. 2000). The error bars on the mean linestrength in a given zone are omitted for clarity as they are smaller or similar to the size of the symbols in the diagrams.

rises to  $45 \text{ km s}^{-1}$  at  $r = 7''$ , and remains constant at larger radii. The velocity field of the main body is not symmetric about the minor axis and the loci of zero velocity (shown as bold line in Figure 1b) and maximum velocity, are not perpendicular. We will explore the consequences of this in a later paper presenting dynamical models. The velocity dispersion falls off smoothly from its central maximum of  $275 \text{ km s}^{-1}$ , and the contours of constant dispersion follow the isophotes (Figure 1c). A detailed comparison shows excellent agreement with the SB long-slit data (de Zeeuw et al. 2001).

Figure 1d shows that the distribution of  $\text{Mg } b$  has a central peak, whereas the  $\text{H}\beta$  value is roughly constant across the galaxy (Figure 1e). Our average value for the central  $\text{H}\beta$  absorption strength is  $1.61 \pm 0.04 \text{ \AA}$ , in good agreement with the Lick/IDS measurement of  $1.66 \pm 0.21 \text{ \AA}$  (Trager et al. 1998). Furthermore, we find no indication for either  $[\text{OIII}]\lambda 5007$  or  $\text{H}\beta$ -emission in our spectra, so there is no evidence that our age estimates are affected by nebular emission.

In Figure 2a we show the  $[\text{MgFe52}]$  vs  $\text{H}\beta$  age-metallicity diagnostic diagram ( $[\text{MgFe52}] = \sqrt{\text{Mg } b \times \text{Fe5270}}$ ). In order to probe the stellar populations of the decoupled core with respect to the main galaxy we have averaged the line-strength in certain key regions (see also Figure 1, enlarged core region). The very central region ( $r < 1''.6$ ) of the galaxy is represented by an open circle. Furthermore, we have identified the decoupled core using the velocity maps and plot the average value for the line-strengths in this region as an open diamond. Comparing this with the average line-strengths of the main galaxy at the *same* radius along the minor axis (open square) we find that these two kinematically distinct regions have identical stellar populations. At larger radii ( $r > 5''.0$ ) we averaged

all lenslets in elliptical annuli (filled circles). The metal line-strength decreases with increasing radius and there is a small increase in  $\text{H}\beta$  absorption strength.

In order to make age and metallicity estimates, we use the Vazdekis (1999) models, which utilize the empirical stellar library of Jones (1997) to predict line-strengths for a single-burst stellar population as a function of age and metallicity. The models were smoothed to the Lick/IDS resolution and include improved stellar population parameters (Vazdekis 2001, in preparation). The model predictions are shown in Figure 2a & c. The central metallicity is estimated to be  $1.15 Z_{\odot}$ , decreasing towards larger radii ( $\approx 0.3$  dex per dex in radius) at a roughly constant age of 14 Gyr (Figure 2a). We note that the absolute age calibration of the models remains subject to systematic errors, but all our conclusions are based on relative age differences which are much more robust. The small increase in  $\text{H}\beta$  absorption at the very center ( $r \lesssim 1''.6$ ) suggests a luminosity-weighted age of  $\approx 12$  Gyr. We can account for this by superimposing a younger population on that of the main body: 6% of the mass in a stellar population with the same metallicity and an age of 5 Gyrs is sufficient.

Figure 2b shows the  $\text{Mg } b - \sigma$  relation within NGC 4365. The central data points agree well with the relation for the cores of early-type galaxies (Colless et al. 1999), suggesting that the core properties of NGC 4365 are similar to those of other ellipticals. For  $r \lesssim 6''$ , the local  $\text{Mg } b - \sigma$  relation shows a steeper slope than the global relation, but overall the gradient in this diagram is typical of similar galaxies studied by Davies, Sadler, & Peletier (1993) and Carollo & Danziger (1994).

In Figure 2c we plot  $\text{Mg } b$  vs  $\text{Fe5270}$ . Stellar population models (Vazdekis 1999) at solar abundance ratios and for ages 12.6 and 17.8 Gyr are overplotted. In

these coordinates the effects of age and metallicity are almost completely degenerate hence the model predictions overlap. Consistent with other giant ellipticals (see e.g., Kuntschner 1998; Kuntschner et al. 2001), the data points for NGC 4365 lie off the solar ratio models towards larger values of Mg  $b$  and lower Fe5270 line-strength. Using the corrections given by Trager et al. (2000) we also plot stellar population models at [Mg/Fe] = 0.22 dex, which are a good representation of the whole of NGC 4365. There is no difference between the decoupled core region and the main body of the galaxy. SB find that the magnesium-to-iron ratio is further enhanced in the very center. Our data, whilst marginally consistent with theirs, indicate no additional enhancement.

#### 4. DISCUSSION

We now explore how the SAURON two-dimensional line-strength maps constrain the star formation history of both the main body and the core of NGC 4365. There is a dramatic difference in the kinematics of the two regions of the galaxy, but other properties suggest that NGC 4365 is a normal elliptical galaxy and that the core and main body had a common star formation history. Furthermore, the K-band surface brightness fluctuations in NGC 4365 place it amongst the old metal-rich ellipticals (Jensen, Tonry, & Luppino 1998).

The elevated magnesium-to-iron ratio is roughly constant across the entire galaxy (a region of  $4 \times 3$  kpc). Such non-solar abundance ratios arise in populations enriched primarily with the products of Type II supernovae, either in a rapid initial burst of star formation or one skewed to massive stars (Worthey 1998). The uniformity of the elevated magnesium-to-iron ratio also suggests that the whole galaxy experienced a common star formation history, involving considerable gaseous dissipation, thus generating the high central metallicity and inward metallicity gradient. A possible formation scenario would be the merger of gas-rich fragments at high redshift. Such an event would be modest compared to the rates of star formation inferred for high-redshift sub-millimeter galaxies (e.g., Ivison et al. 2000). The decoupled core could originate from stars ejected into a tidal tail (with the appropriate angular momentum) as a result of a major merger that formed the bulk of the stars. These stars fall back to produce the kinematically distinct component at the centre.

If star formation was taken to completion and the residual gas exhausted roughly 12 Gyr ago, then the decoupled kinematic structure in NGC 4365 must be long-lived.

The misalignment of the kinematic and photometric axes show that the main body of the galaxy is triaxial, with the bulk of its stars on long-axis tubes and the stars in the core predominantly on short-axis tubes (Statler 1991; Arnold, de Zeeuw, & Hunter 1994). This is similar to the structure inferred for, e.g., NGC 4261 (Davies & Birkinshaw 1986) and NGC 4406 (Franx, Illingworth, & Heckman 1989). The full two-dimensional structure and kinematics derived from the SAURON data, when combined with our dynamical models (see e.g., Cretton et al. 1999), will enable us to distinguish between a thin disk or a thick structure for the core.

#### 5. CONCLUSIONS

The SAURON maps present a complete view of the kinematics and stellar populations of NGC 4365. They show two independent kinematic subsystems: the central  $300 \times 700$  pc and the main body of the galaxy, rotating almost at right angles to each other. The misalignment of  $82^\circ$  between the photometric and kinematic axes of the main body is unambiguous evidence of triaxiality. The SAURON maps enable us to compare the stellar population in the decoupled component with that in the main body of the galaxy at the same radius. We find these populations to be indistinguishable in age, metallicity and abundance ratios. We find an age of  $\approx 14$  Gyr and a decrease in metallicity, from larger than solar in the center to half solar at a radius of 2 kpc ( $\approx 0.4 r_e$ ). We suggest that NGC 4365 underwent dissipative star formation at high redshift, probably through one or more mergers. Later generations of stars formed a more centrally-concentrated, metal-enriched stellar population. Star formation was complete and the residual gas was exhausted roughly 12 Gyr ago. This also suggests that the observed kinematics and triaxial structure is stable.

It is a pleasure to thank Rene Rutten and the ING staff, in particular Tom Gregory, for support on La Palma. We thank Richard McDermid for assistance during the observing run. The SAURON project is made possible through grants 614.13.003 and 781.74.203 from ASTRON/NWO, PPARC grant “Extragalactic Astronomy & Cosmology at Durham 1998-2002” and financial contributions from the Institut National des Sciences de l’Univers, the Université Claude Bernard Lyon I, together with the universities of Durham and Leiden. RLD gratefully acknowledges the award of a Research Fellowship from the Leverhulme Trust.

#### REFERENCES

Arnold, R. A., de Zeeuw, P. T., & Hunter, C. 1994, MNRAS, 271, 924  
 Bacon, R., et al. 2001, MNRAS, submitted  
 Bender, R. 1988, A&A, 202, L5  
 Bender, R. 1990, A&A, 229, 441  
 Bender, R., Saglia, R. P., & Gerhard, O. E. 1994, MNRAS, 269, 785  
 Burstein, D., Davies, R. L., Dressler, A., Faber, S. M., Stone, R. P. S., Lynden-Bell, D., Terlevich, R. J., & Wegner, G. 1987, ApJS, 64, 601  
 Carollo, C. M., & Danziger, I. J. 1994, MNRAS, 270, 523  
 Carollo, C. M., Franx, M., Illingworth, G. D., & Forbes, D. 1997, ApJ, 481, 710  
 Colless, M., Burstein, D., Davies, R. L., McMahan, R. K., Saglia, R. P., & Wegner, G. 1999, MNRAS, 303, 813  
 Cretton, N., de Zeeuw, P. T., van der Marel, R. P., & Rix, H. 1999, ApJS, 124, 383  
 Davies, R. L., & Birkinshaw, M. 1986, ApJ, 303, L45  
 Davies, R. L., Sadler, E. M., & Peletier, R. F. 1993, MNRAS, 262, 650  
 van Dokkum, P. G., & Franx, M. 1995, AJ, 110, 2027  
 Franx, M., & Illingworth, G. D. 1988, ApJ, 327, L55  
 Franx, M., Illingworth, G., & Heckman, T. 1989, ApJ, 344, 613  
 Hau, G. K. T., Carter, D., & Balcells, M. 1999, MNRAS, 306, 437  
 Ivison, R. J., Smail, I., Barger, A. J., Kneib, J., Blain, A. W., Owen, F. N., Kerr, T. H., & Cowie, L. L. 2000, MNRAS, 315, 209  
 Jensen, B. J., Tonry, J. L., & Luppino, G. A. 1998, ApJ, 505, 111  
 Jones, L. A. 1997, PhD Thesis, University of North Carolina, Chapel Hill

Kuntschner, H. 1998, PhD thesis, University of Durham

Kuntschner, H., Lucey, J. R., Smith, S. J., Hudson, M. J., & Davies, R. L. 2001, MNRAS, accepted

Rix, H.-W., & White, S. D. M. 1992, MNRAS, 254, 389

Statler, T. S. 1991, ApJ, 382, L11

Surma, P., & Bender, R. 1995, A&A, 298, 405 (SB)

Trager, S. C., Worthey, G., Faber, S. M., Burstein, D., & Gonzalez, J. J. 1998, ApJS, 116, 1

Trager, S. C., Faber, S. M., Worthey, G., & González, J. J. 2000, AJ, 119, 1645

Vazdekis, A. 1999, ApJ, 513, 224

Wagner, S. J., Bender, R., & Möllenhoff, C. 1988, A&A, 195, L5

Worthey, G. 1994, ApJS, 95, 107

Worthey, G. 1998, PASP, 110, 888

de Zeeuw, P. T., & Franx, M. 1991, ARAA, 29, 239

de Zeeuw, P. T., et al. 2001, MNRAS, submitted